Electronic Structure of $[Pt_2(\mu\text{-}O_2CCH_3)_4(H_2O)_2]^{2+}$ Using the Quasi-Relativistic Xα−SW Method: Analysis of Metal−Metal Bonding, Assignment of Electronic Spectra, and Comparison with $Rh_2(\mu\text{-}O_2CCH_3)_4(H_2O)_2$

Robert Stranger,*,† Gregory A. Medley,‡ John E. McGrady,† Jodie M. Garrett,‡ and Trevor G. Appleton‡

Departments of Chemistry, The Australian National University, Canberra, ACT 0200, Australia, and The University of Queensland, Brisbane, QLD 4072, Australia

Received May 16, 1995[⊗]

The electronic structure and metal−metal bonding in the classic d^7d^7 tetra-bridged *lantern* dimer $[Pt_2(O_2CCH_3)_4(H_2O)_2]^{2+}$ has been investigated by performing quasi-relativistic Xα−SW molecular orbital calculations on the analogous formate-bridged complex. From the calculations, the highest occupied and lowest unoccupied metal-based levels are $\delta^*(Pt_2)$ and $\sigma^*(Pt_2)$, respectively, indicating a metal−metal single bond analogous to the isoelectronic Rh(II) complex. The energetic ordering of the main metal−metal bonding levels is, however, quite different from that found for the Rh(II) complex, and the upper metal−metal bonding and antibonding levels have significantly more ligand character. As found for the related complex $[W_2(O_2CH)_4]$, the inclusion of relativistic effects leads to a further strengthening of the metal−metal σ bond as a result of the increased involvement of the higher-lying platinum 6s orbital. The low-temperature absorption spectrum of $[Pt_2(O_2CCH_3)_4(H_2O)_2]^{2+}$ is assigned on the basis of Xα−SW calculated transition energies and oscillator strengths. Unlike the analogous Rh(II) spectrum, the visible and near-UV absorption spectrum is dominated by charge transfer (CT) transitions. The weak, visible bands at 27 500 and 31 500 cm^{-1} are assigned to Ow → $\sigma^*(Pt_2)$ and OAc → $\sigma^*(Pt_2)$ CT transitions, respectively, although the donor orbital in the latter transition has around 25% $\pi^*(Pt_2)$ character. The intense near-UV band around 37 500 cm^{-1} displays the typical lower energy shift as the axial substituents are changed from H_2O to Cl and Br, indicative of significant charge transfer character. From the calculated oscillator strengths, a number of transitions, mostly OAc → σ^*(Pt−O) CT in nature, are predicted to contribute to this band, including the metal-based $\sigma(Pt_2) \rightarrow \sigma^*(Pt_2)$ transition. The close similarity in the absorption spectra of the CH_3COO^-, SO_4^{2-}, and HPO_4^{2-} bridged Pt(III) complexes suggests that analogous spectral assignments should apply to $[Pt_2(SO_4)_4(H_2O)_2]^{2-}$ and $[Pt_2(HPO_4)_4(H_2O)_2]^{2-}$. Consequently, the anomalous MCD spectra reported recently for the intense near-UV band in the SO_4^{2-} and HPO_4^{2-} bridged Pt(III) complexes can be rationalized on the basis of contributions from either $SO_4 \rightarrow \sigma^*$(Pt−O) or $HPO_4 \rightarrow \sigma^*$(Pt−O) CT transitions. The electronic absorption spectrum of $[Rh_2(O_2CCH_3)_4(H_2O)_2]$ has been re-examined on the basis of Xα−SW calculated transition energies and oscillator strengths. The intense UV band at ∼45 000 cm^{-1} is predicted to arise from several excitations, both metal-centered and CT in origin. The lower energy shoulder at approximately 40 000 cm^{-1} is largely attributed to the metal-based $\sigma(Rh_2) \rightarrow \sigma^*(Rh_2)$ transition.

Introduction

The dinuclear tetracarboxylate bridged *lantern* complexes, $M_2(\mu\text{-}O_2CR)_4L_2$ are known for many metal ions, including V, Cr, Mo, W, Re, Co, Cu, Tc, Ru, and Rh.[1,2] Surprisingly, although the related d^7d^7 dinuclear *lantern* complexes of Pt(III) involving bridging sulfate (SO_4^{2-}), hydrogen phosphate (HPO_4^{2-}), and pyrophosphite ($H_2P_2O_5^{2-}$) ligands are well-known, the tetraacetate complexes $Pt_2(O_2CCH_3)_4L_2$ have only recently been prepared and characterized.[3,4] On the basis of the rather short metal−metal distance of 2.390(1) Å found[3] for $[Pt_2(O_2CCH_3)_4(H_2O)_2]^{2+}$ compared to the analogous SO_4^{2-}, HPO_4^{2-}, and $H_2P_2O_5^{2-}$ bridged complexes, it now appears that the earlier difficulty in isolating these Pt(III) species was due to the strain induced in adopting the *lantern* structure. For $[Pt_2(O_2CCH_3)_4(H_2O)_2]^{2+}$, the Pt(III) metal ions are displaced inwards from their PtO_4 plane toward one another by approximately 0.07 Å. These Pt(III) dimers are isoelectronic with their Rh(II) analogues, which, from electronic structure calculations, are known to possess a metal−metal σ bond arising from the $\sigma^2\pi^4\delta^2\pi^{*4}\delta^{*2}$ orbital configuration.

In comparison with the isoelectronic Rh(II) complexes, $Rh_2(O_2CR)_4L_2$, the increased charge on the Pt(III) metal ion should result in a stabilization of the metal d orbitals relative to the ligand donor orbitals, and consequently, the likelihood of greater mixing between metal and ligand based orbitals. The effect of this mixing on the metal−metal bonding interaction is of some interest. In addition, the inclusion of relativistic effects in the electronic structure calculation of the related tungsten(II) complexes, $W_2(O_2CH_3)_4$ and $W_2(O_2CH_3)_4(CH_3)_2$, revealed a significant contribution from the tungsten 6s orbital to the metal−metal σ bond.[5] It remains to be seen whether a similar effect occurs in the Pt(III) analogue.

* Author to whom correspondence should be addressed.
† The Australian National University.
‡ The University of Queensland.
⊗ Abstract published in *Advance ACS Abstracts,* February 15, 1996.
(1) Cotton, F. A.; Walton, R. A. *Multiple Bonds Between Metal Atoms*, 2nd ed.; Oxford University Press: New York, 1993.
(2) Cotton, F. A.; Walton, R. A. *Struct. Bonding* **1985**, *62*, 1.
(3) Appleton, T. G.; Byriel, K. A.; Hall, J. R.; Kennard, C. H. L.; Mathieson, M. T. *J. Am. Chem. Soc.* **1992**, *114*, 7305.
(4) Appleton, T. G.; Byriel, K. A.; Garrett, J. M.; Hall, J. R.; Kennard, C. H. L.; Mathieson, M. T.; Stranger, R. *Inorg. Chem.* **1995**, *34*, 5646.

0020-1669/96/1335-2268$12.00/0

The electronic spectra of Pt(III) *lantern* complexes $[Pt_2(pop)_4L_2]^{n-}$ (pop = $H_2P_2O_5^{2-}$) have been extensively investigated.[6−11] More recently, detailed electronic spectroscopy studies of the sulfate $[Pt_2(SO_4)_4L_2]^{n-}$ and hydrogen phosphate complexes $[Pt_2(HPO_4)_4L_2]^{n-}$ have been reported.[12−14] We have also reported the electronic spectra of the Pt(III) complexes $[Pt_2(O_2CCH_3)_4L_2]^{n-}$ (L = Cl, Br, OAc, H_2O)[4] and found their spectra to be very similar to the sulfate and hydrogen phosphate bridged counterparts. The analysis and assignment of the electronic spectra of all of these Pt(III) complexes has relied heavily on the electronic structure determined for the isoelectronic rhodium(II) complexes $Rh(O_2CH_3)_4L_2$ (L = H_2O, PH_3) from Xα−SW calculations.[15,16] However, the very recent MCD analysis of the $[Pt_2(SO_4)_4L_2]^{4-}$ and $[Pt_2(HPO_4)_4L_2]^{4-}$ (L = H_2O, Cl, Br) complexes[14] is in conflict with certain of these assignments, in particular, the location of the intense $\sigma(Pt_2,L) \rightarrow \sigma^*(Pt_2)$ transition.

In order to investigate the electronic structure and metal−metal bonding in $Pt_2(\mu\text{-}O_2CCH_3)_4L_2$ complexes, we now present the results of electronic structure calculations on the analogous formate-bridged complex $[Pt_2(\mu\text{-}O_2CH)_4(H_2O)_2]^{2+}$ using the quasi-relativistic Xα−SW method.[29] In addition, the calculated transition energies and oscillator strengths are reported for this complex and the isoelectronic rhodium(II) complex $[Rh_2(O_2CH)_4(H_2O)_2]$ in order to provide a more reliable basis for assigning the electronic spectra of these and the related sulfate and phosphate bridged complexes.

Table 1. Structural Parameters Used in Xα−SW Calculations

Distances		
structural param	$[Pt_2(O_2CH)_4(H_2O)_2]^{2+}$	$[Rh_2(O_2CH)_4(H_2O)_2]$
M−M (Å)	2.390	2.385
M−O (Å)	2.007	2.039
M−OH_2 (Å)	2.167	2.310
C−O (Å)	1.268	1.269
C−H (Å)	1.08	1.08
H−OH (Å)	0.99	0.99
Angles		
structural param	$[Pt_2(O_2CH)_4(H_2O)_2]^{2+}$	$[Rh_2(O_2CH)_4(H_2O)_2]$
M−M−O (deg)	88.1	88.1
O−C−O (deg)	126.2	124.8
H−O−H (deg)	120.0	120.0

Experimental Sections

Xα−SW Calculations. Spin-restricted self-consistent-field Xα−scattered wave (SCF−Xα−SW)[27,28] calculations were performed on a DEC 5000/240 work station using a modified version of the XASW Fortran program written by Cook and Case.[29] Geometries for $[Pt_2(O_2CH)_4(H_2O)_2]^{2+}$ and $[Rh_2(O_2CH)_4(H_2O)_2]$ were based on the reported single crystal structures[4,30] of their acetate analogues but idealized to D_{2h} symmetry using the bond lengths and angles given in Table 1. Atomic sphere radii were chosen using the Norman criteria.[31,32] The α values used in the atomic regions were those determined by Schwartz,[33,34] while those used in the inter- and outer-sphere regions were weighted averages of the atomic α values. The molecular *x* axis was orientated along the metal−metal direction with the *xz* plane containing both axial water ligands but dihedral with respect to the bridging formate groups. This orientation of the axial water ligands enabled the SCF refinements to be carried out for D_{2h} molecular symmetry. The wave functions were expanded in spherical harmonics out to $l = 5$ on the outer-sphere, $l = 5$ on the Pt and Rh atoms, $l = 4$ on the O and C atoms, and $l = 1$ on the H atoms. Expansion of the wave functions out to these *l* values was necessary in order to achieve reasonable convergence of calculated oscillator strengths. A Watson sphere of 2− charge coincident with the outer-sphere radius was used to account for the positive charge of the Pt complex. A quasi-relativistic correction using the method of Boring and Wood[37] was applied to both the core and valence electrons of platinum. A calculation for $[Pt_2(O_2CH)_4(H_2O)_2]^{2+}$ without any relativistic correction was also undertaken to determine the extent of relativistic effects. The orbital levels for the component fragments $[Pt_2]$ and $(H_2O)_2$ were not determined from separate SCF calculations but were obtained *in situ* from the converged potential for $[Pt_2(O_2CH)_4(H_2O)_2]^{2+}$ using the procedure described by Bursten and Cotton.[16] Transition energies within the ground state spin manifold were determined using the Slater transition state method,[27] while oscillator strengths were calculated using the method of Noodleman *et al*.[35]

Absorption Spectra. Absorption spectra were measured on a Cary-17 spectrophotometer modified to allow data acquisition and control by an external computer. Low-temperature (∼10 K) spectra of the $[Pt_2(O_2CCH_3)_4(H_2O)_2]^{2+}$ complex in nafion film (Aldrich Nafion 117 perfluorinated membrane, 0.0007-in. thick) were obtained using a Leybold Heraeus ROK 10−300 closed-cycle helium cryostat system. The software packages *SpectraCalc* (Galactic Industries) and *SigmaPlot* (Jandel Scientific) were used for spectral analysis and plotting.

(5) Braydich, M. D.; Bursten, B. E.; Chisholm, M. H.; Clark, D. L. *J. Am. Chem. Soc.* **1985**, *107*, 4459.
(6) Isci, H.; Mason, W. R. *Inorg. Chem.* **1985**, *24*, 1761.
(7) Che, C.-M.; Butler, L. G.; Grunthaner, P. J.; Gray, H. B. *J. Am. Chem. Soc.* **1985**, *107*, 4662.
(8) Che, C.-M.; Mak, T. C. W.; Miskowski, V. M.; Gray, H. B. *J. Am. Chem. Soc.* **1986**, *108*, 7840.
(9) Che, C.-M.; Cho, K.-C.; Chan, W.-S. *Inorg. Chem.* **1986**, *25*, 4906.
(10) Stiegman, A. E.; Miskowski, V. M.; Gray, H. B. *J. Am. Chem. Soc.* **1986**, *108*, 2781.
(11) Che, C.-M.; Lee, W.-M.; Cho, K.-C. *J. Am. Chem. Soc.* **1988**, *110*, 5407.
(12) Shin, Y.-g. K.; Miskowski, V. M.; Nocera, D. G. *Inorg. Chem.* **1990**, *29*, 2308.
(13) Newman, R. A.; Martin, D. S.; Dallinger, R. F.; Woodruff, W. H.; Stiegman, A. E.; Che, C.-M.; Schaefer, W. P.; Miskowski, V. M.; Gray, H. B. *Inorg. Chem.* **1991**, *30*, 4647.
(14) Gökagac, G.; Isci, H.; Mason, W. R. *Inorg. Chem.* **1992**, *31*, 2184.
(15) Norman, J. G.; Kolari, H. J. *J. Am. Chem. Soc.* **1978**, *100*, 791.
(16) Bursten, B. E.; Cotton, F. A. *Inorg. Chem.* **1981**, *20*, 3042.
(17) (a) Desjardins, S. J.; Penfield, K. W.; Cohen, S. L.; Musselman, R. L.; Solomon, E. I. *J. Am. Chem. Soc.* **1983**, *105*, 4590. (b) Aizman, A.; Case, D. A. *Inorg. Chem.* **1981**, *20*, 528.
(18) Martin, D. S.; Webb, T. R.; Robbins, G. A.; Fanwick, P. E. *Inorg. Chem.* **1979**, *18*, 475.
(19) Sowa, T.; Kawamura, T.; Shida, T.; Yonezawa, T. *Inorg. Chem.* **1983**, *22*, 56.
(20) Miskowski, V. M.; Schaefer, W. P.; Sadeghi, B.; Santarsiero, B. D.; Gray, H. B. *Inorg. Chem.* **1984**, *23*, 1154.
(21) Trexler, J. W.; Schreiner, A. F.; Cotton, F. A. *Inorg. Chem.* **1988**, *27*, 1.
(22) Klyagina, A. P.; Golovaneva, I. F.; Levin, A. A. *Russ. J. Inorg. Chem.* **1990**, *35*, 1138.
(23) Golovaneva, I. F.; Polonskii, S. A.; Klyagina, A. P. *Russ. J. Inorg. Chem.* **1994**, *39*, 79.
(24) Bursten, B. E.; Clark, D. L. *Polyhedron* **1987**, *6*, 695.
(25) Heath, G. A.; McGrady, J. E. *J. Chem. Soc., Dalton Trans.* **1994**, 3759.
(26) Gheller, S. F.; Heath, G. A.; Hockless, D. C.; Humphrey, D. G.; McGrady, J. E. *Inorg. Chem.* **1994**, *33*, 3986.
(27) Slater, J. C. *The Self-Consistent Field for Molecules and Solids: Quantum Theory of Molecules and Solids*; McGraw-Hill: New York, 1974; Vol. 4.
(28) Johnson, K. H. *Adv. Quantum Chem.* **1973**, *7*, 143.
(29) Cook, M.; Case, D. A. *XASW-A Fortran Program for Atomic X-Alpha and Molecular Multiple Scattering X-Alpha Electronic Structure Calculations*, Version 2, 1982, QCPE Program 465, 1982.
(30) Cotton, F. A.; DeBoer, B. G.; LaPrade, M. D.; Pipal, J. R.; Ucko, D. A. *Acta Crystallogr., Sect. B* **1971**, *27*, 1664.
(31) Norman, J. G., Jr. *J. Chem. Phys.* **1974**, *61*, 4630.
(32) Norman, J. G., Jr. *Mol. Phys.* **1976**, *31*, 1191.
(33) Schwarz, K. *Phys. Rev. B* **1972**, *5*, 2466.
(34) Schwarz, K. *Theor. Chim. Acta* **1974**, *34*, 225.
(35) Noodleman, L. *J. Chem. Phys.* **1976**, *64*, 2343.
(36) Hopkins, M. D.; Gray, H. B.; Miskowski, V. M. *Polyhedron* **1987**, *6*, 705.
(37) Wood, J. H.; Boring, A. M. *Phys. Rev. B* **1978**, *18*, 2701.

Table 2. Upper Valence Energy Levels and Their Composition for $[Pt_2(O_2CH)_4(H_2O)_2]^{2+}$

		composn (%)			
level	energy (eV)	Pt_2	$(O_2CH)_4$	$(H_2O)_2$	orbital description
$6b_{3g}$	−8.2839	40	60	0	σ^*(Pt−O)
$5a_u$	−8.9490	47	53	0	σ^*(Pt−O)
$8b_{3u}$	−9.5564	60	21	19	$\sigma^*(Pt_2)$, σ^*(Pt−O)
$6b_{1g}$	−11.7509	14	3	83	Ow lone pair
$7b_{2u}$	−11.8516	5	16	79	Ow lone pair
$7b_{3u}$	−11.9444	35	65	0	O lone pair, $\delta^*(Pt_2)$
$7b_{1u}$	−12.2671	7	93	0	O lone pair
$6b_{2u}$	−12.3425	4	83	13	O lone pair
$6b_{2g}$	−12.6921	31	69	0	O lone pair, $\pi^*(Pt_2)$
$4a_u$	−12.7133	0	100	0	O lone pair
$5b_{1g}$	−12.7916	17	76	7	O lone pair, $\pi^*(Pt_2)$
$9a_g$	−12.9295	26	28	46	σ^*(Pt−Ow), $\sigma(Pt_2)$
$5b_{2g}$	−13.1356	7	93	0	O lone pair
$4b_{1g}$	−13.1733	7	90	3	O lone pair
$8a_g$	−13.1818	53	47	0	$\delta(Pt_2)$
$7a_g$	−14.0560	15	62	23	σ(Pt−O), σ^*(Pt−Ow)
$4b_{2g}$	−14.2242	64	35	1	$\pi^*(Pt_2)$, σ(Pt−O)
$3b_{1g}$	−14.3558	66	29	5	$\pi^*(Pt_2)$, σ(Pt−O)
$5b_{3g}$	−14.3963	0	100	0	O lone pair
$6b_{3u}$	−14.4334	11	68	21	O lone pair
$6b_{1u}$	−14.7507	14	86	0	O lone pair
$4b_{3g}$	−14.7576	27	73	0	O lone pair
$5b_{2u}$	−14.7716	8	92	0	O lone pair
$5b_{1u}$	−15.0745	57	43	0	$\pi(Pt_2)$, π(CO)
$4b_{2u}$	−15.1387	59	40	1	$\pi(Pt_2)$, π(CO)
$3a_u$	−15.2548	27	73	0	σ(Pt−O)
$5b_{3u}$	−15.7076	67	33	0	$\delta^*(Pt_2)$, σ(Pt−O)
$4b_{3u}$	−15.8820	29	11	60	σ(Pt−Ow), $\sigma^*(Pt_2)$
$6a_g$	−16.5457	48	52	0	$\delta(Pt_2)$, π(Pt−O)
$5a_g$	−17.0154	6	93	1	π(CO)
$4b_{1u}$	−17.1017	22	77	1	π(CO), $\pi(Pt_2)$
$3b_{3g}$	−17.1103	11	89	0	π(CO)
$3b_{2u}$	−17.1249	23	77	0	π(CO), $\pi(Pt_2)$
$4a_g$	−17.6243	68	5	27	$\sigma(Pt_2)$, σ(Pt−Ow)

Results and Discussion

Electronic Structure of $[Pt_2(O_2CH)_4(H_2O)_2]^{2+}$. The upper valence energy levels and their composition determined from the relativistic calculation of $[Pt_2(O_2CH)_4(H_2O)_2]^{2+}$ and a nonrelativistic calculation of $[Rh_2(O_2CH)_4(H_2O)_2]$ are given in Tables 2 and 3, respectively. The energy levels calculated for the Rh(II) complex are very similar to those obtained by Norman and Kolari,[15] the differences being largely attributable to the expansion of the wave functions out to higher *l* values in our calculations. The energy levels for the Pt(III) complex, together with those obtained from a nonrelativistic calculation, are plotted in Figure 1 except for levels which are predominantly localized on either the formate or axial water ligands. The molecular orbitals involved in Pt−Pt bonding or antibonding interactions for $[Pt_2(O_2CH)_4(H_2O)_2]^{2+}$ are compared with those of its component fragments $[Pt_2]$ and $(H_2O)_2$ in Figure 2. The orbital levels for these component fragments were not determined from separate SCF calculations but instead were obtained *in situ* from the refined potential for $[Pt_2(O_2CH)_4(H_2O)_2]^{2+}$. In this way the fragment energy levels can be directly compared with those of $[Pt_2(O_2CH)_4(H_2O)_2]^{2+}$. The energy levels obtained from the relativistic calculation of $[Pt_2(O_2CH)_4(H_2O)_2]^{2+}$ are compared with those calculated for the analogous Rh(II) complex in Figure 3, where the Rh(II) levels have been adjusted so that the $4a_u$ orbitals, which are localized entirely on the formate groups, coincide energetically in both complexes. Finally, contour maps for the orbitals involved in significant Pt−Pt bonding or antibonding interactions are shown in Figure 4.

From Table 2, the highest occupied ($7b_{3u}$) and lowest unoccupied ($8b_{3u}$) metal-based levels in $[Pt_2(O_2CH)_4(H_2O)_2]^{2+}$ correspond to $\delta^*(Pt_2)$ and $\sigma^*(Pt_2)$ respectively, analogous to the isoelectronic Rh(II) complex. Energetically though, the HOMO levels are calculated to be the $6b_{1g}$ and $7b_{2u}$ orbitals, which correspond predominantly to oxygen lone pair orbitals

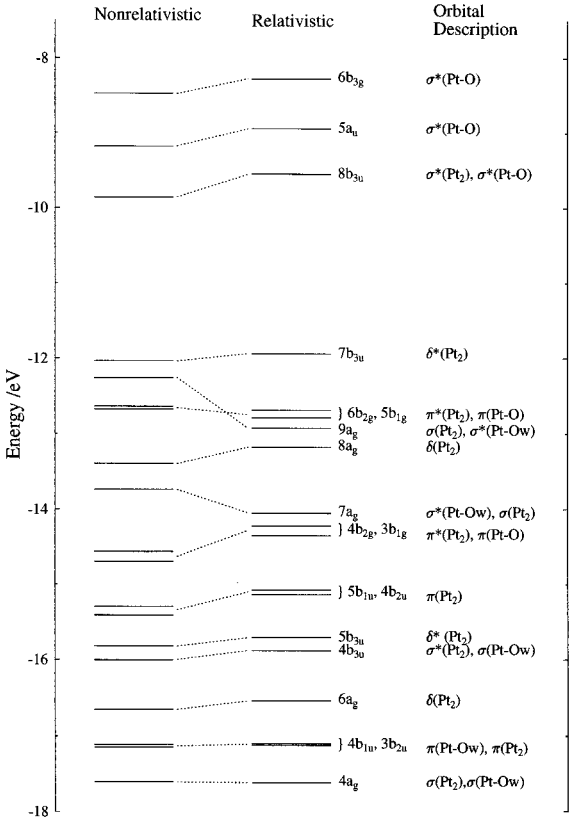

Figure 1. Upper valence energy levels and orbital descriptions for $[Pt_2(O_2CH)_4(H_2O)_2]^{2+}$ based on quasi-relativistic and nonrelativistic Xα−SW calculations.

Table 3. Upper Valence Energy Levels and Their Composition for $[Rh_2(O_2CH)_4(H_2O)_2]$

		orbital composn (%)			
level	energy (eV)	Rh_2	$(O_2CH)_4$	$(H_2O)_2$	orbital description
$6b_{3g}$	−5.2219	53	47	0	σ^*(Rh−O)
$5a_u$	−5.6736	58	42	0	σ^*(Rh−O)
$8b_{3u}$	−6.1539	74	18	8	$\sigma^*(Rh_2)$, σ^*(Rh−Ow)
$7b_{3u}$	−8.2165	65	35	0	$\delta^*(Rh_2)$,
$6b_{1g}$	−8.3471	75	11	14	$\pi^*(Rh_2)$,
$6b_{2g}$	−8.5389	84	16	0	$\pi^*(Rh_2)$,
$9a_g$	−9.0587	80	20	0	$\delta(Rh_2)$,
$7b_{2u}$	−9.0614	25	28	47	π(Rh−O), $\pi(Rh_2)$
$7b_{1u}$	−9.3512	30	70	0	π(Rh−O), $\pi(Rh_2)$
$8a_g$	−9.4260	50	32	18	$\sigma(Rh_2)$, σ^*(Rh−Ow)
$5b_{1g}$	−9.5213	8	18	74	Ow lone pair
$6b_{2u}$	−9.5947	7	57	36	Ow lone pair
$4a_u$	−9.8451	0	100	0	O lone pair
$5b_{2g}$	−10.1716	5	95	0	O lone pair
$4b_{1g}$	−10.2029	6	91	3	O lone pair
$4b_{2g}$	−10.4696	13	87	0	O lone pair
$3b_{1g}$	−10.4927	15	83	2	O lone pair
$6b_{1u}$	−10.5880	63	37	0	$\pi(Rh_2)$, π(Rh−O)
$5b_{2u}$	−10.6696	63	32	5	$\pi(Rh_2)$, π(Rh−O)
$6b_{3u}$	−10.9907	11	79	10	σ,π(Rh−O)
$7a_g$	−11.0369	17	68	15	σ,π(Rh−O)
$3a_u$	−11.5349	25	75	0	σ,π(Rh−O)
$5b_{3g}$	−11.6029	32	68	0	σ,π(Rh−O)
$5b_{3u}$	−11.6029	35	65	0	σ,π(Rh−O)
$4b_{3g}$	−11.7131	0	100	0	π(CO)
$4b_{3u}$	−12.1268	14	15	71	σ(Rh−Ow), $\sigma^*(Rh_2)$
$4b_{2u}$	−12.1526	1	99	0	π(CO)
$5b_{1u}$	−12.1526	1	99	0	π(CO)
$6a_g$	−12.6846	41	11	48	σ(Rh−Ow), $\sigma(Rh_2)$
$5a_g$	−13.0465	17	83	0	π(Rh−OC)

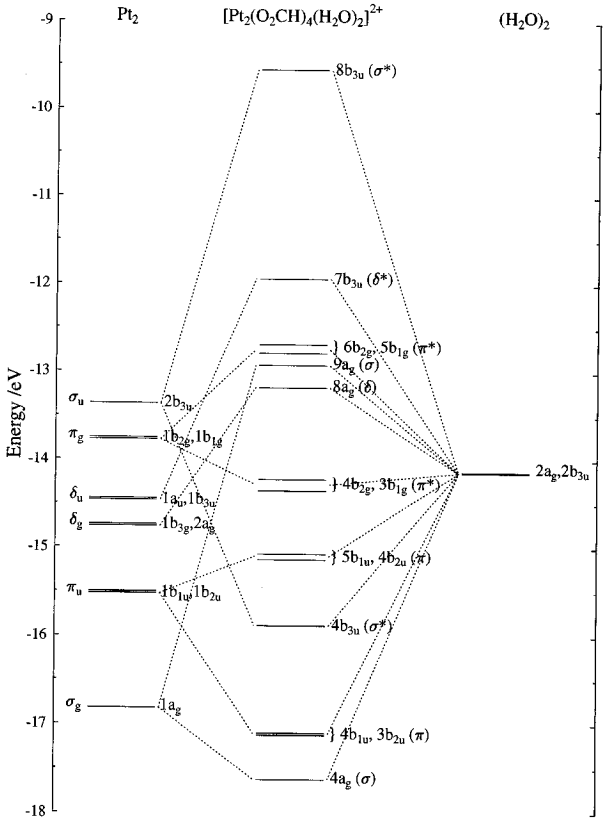

Figure 2. Comparison of upper valence energy levels involved in Pt−Pt bonding for $[Pt_2(O_2CH)_4(H_2O)_2]^{2+}$, Pt_2, and $(H_2O)_2$. Energy levels for the component fragments Pt_2 and $(H_2O)_2$ were determined *in situ* from the converged potential for $[Pt_2(O_2CH)_4(H_2O)_2]^{2+}$.

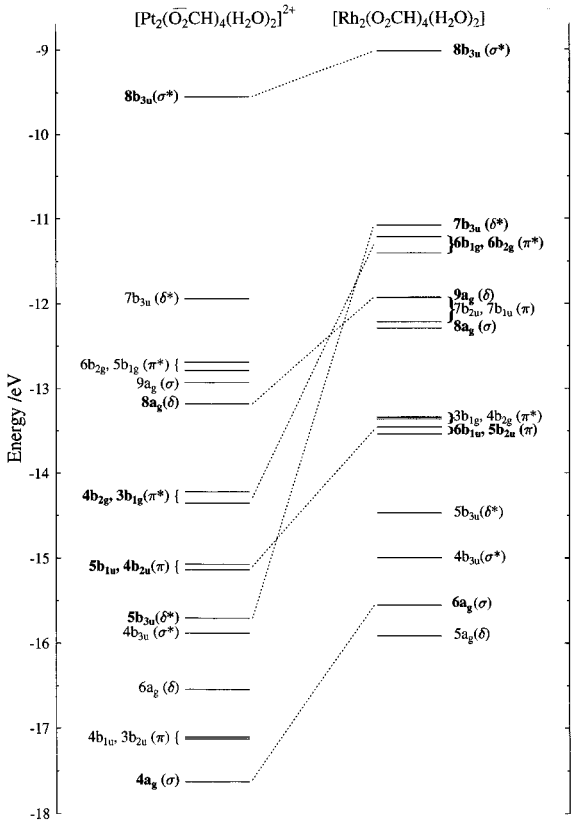

Figure 3. Comparison of upper valence energy levels involved in metal−metal bonding in $[Pt_2(O_2CH)_4(H_2O)_2]^{2+}$ and $[Rh_2(O_2CH)_4(H_2O)_2]$. The energy levels shown for $[Rh_2(O_2CH)_4(H_2O)_2]$ have been adjusted so that the $4a_u$ orbitals, which are localized entirely on the formate groups, coincide energetically in both complexes. Main σ, π, and δ metal-based levels are shown in bold type.

localized on the axial water ligands. However, given the number of other levels which lie energetically close to these two orbitals, in particular the $7b_{3u}$ $\delta^*(Pt_2)$ orbital, and the well-known fact[17] that the SCF−Xα−SW method overestimates the stability of the metal d orbitals, it is arguable whether the $6b_{1g}$ and $7b_{2u}$ levels are the true HOMOs. The analogous oxygen (water) lone pair orbitals in the isoelectronic Rh(II) complex lie well below the $\delta^*(Rh_2)$ HOMO level. The fact that these three levels lie closer together in the Pt(III) complex is not surprising since the increased charge on the platinum will result in a stabilization of the metal d-orbitals relative to the Rh(II) complex. This is borne out by the fact that the energy difference between the axial water lone pair ($6b_{1g}$, $7b_{3u}$) levels and the $4a_u$ level, which is almost 100% localized on the O_2CH fragment, is very similar in both complexes.

From the composition of the upper valence levels for $[Pt_2(O_2CH)_4(H_2O)_2]^{2+}$ given in Table 2, it is apparent that significant mixing of the Pt metal−metal bonding and antibonding orbitals with both the axial water and equatorial formate levels has occurred. Consequently, unlike the isoelectronic Rh(II) analogue, the upper Pt(III) metal−metal bonding and antibonding orbitals have significantly more ligand character, making the identification of the major metal−metal σ, π, and δ bonding and antibonding levels more difficult. For example, in $[Rh_2(O_2CH)_4(H_2O)_2]$, the $7b_{3u}$ $\delta^*(Rh_2)$ level is predominantly localized on the metals (70% Rh character) with a smaller contribution from the formate groups (30% O_2CH character), whereas in $[Pt_2(O_2CH)_4(H_2O)_2]^{2+}$ this same level has a significantly smaller contribution from the metals (35% Pt character) and a much larger contribution from the formate groups (62% O_2CH character).

Although the overall metal−metal bonding picture is less clear in $[Pt_2(O_2CH)_4(H_2O)_2]^{2+}$, a comparison of the metal−metal σ bonding and antibonding levels for the $[Pt_2]$ fragment with those for $[Rh_2]$[15,16] clearly indicates that the metal-metal σ bond is stronger in the Pt(III) complex. This is also borne out from a comparison of the metal−metal σ bonding and antibonding orbitals in the Pt(III) and Rh(II) complexes shown in Figure 3, where the major σ, π, and δ metal-based levels, on the basis of percentage contribution of metal character, are indicated in bold type. For $[Pt_2(O_2CH)_4(H_2O)_2]^{2+}$ the $\sigma(Pt_2)-\sigma^*(Pt_2)$ ($4a_g-8b_{3u}$) separation is approximately 8.1 eV, whereas for $[Rh_2(O_2CH)_4(H_2O)_2]$ the analogous separation ($6a_g-8b_{3u}$) is smaller around 6.5 eV. Also apparent from Figure 3 is that the energetic ordering of the main metal−metal bonding and antibonding levels is quite different in the two complexes. In $[Rh_2(O_2CH)_4(H_2O)_2]$ the ordering is seen to be $\pi^4 < \sigma^2 < \delta^2 < \pi^{*4} < \delta^{*2} < \sigma^*$, whereas in $[Pt_2(O_2CH)_4(H_2O)_2]^{2+}$ the ordering is $\sigma^2 < \delta^{*2} < \pi^4 < \pi^{*4} < \delta^2 < \sigma^*$. The additional stabilization of the Pt(III) d levels compared to those of Rh(II) is also evident from Figure 3. As a consequence, the axial water lone pair (a_g + b_{3u}) levels interact strongly with both $\sigma(Pt_2)$ and $\sigma^*(Pt_2)$ metal−metal bonding levels (see Figure 2). This situation contrasts with that in $[Rh_2(O_2CH)_4(H_2O)_2]$, where a strong interaction only occurs between the a_g axial water σ level and the $\sigma(Rh_2)$ metal−metal bonding levels.

The effect of the quasi-relativistic correction on the valence molecular orbital energies of $[Pt_2(O_2CH)_4(H_2O)_2]^{2+}$ shown in Figure 1, although not as dramatic as that found for the related tungsten(II) complex $W_2(O_2CH)_4$,[5] is qualitatively similar, in agreement with the expected mass−velocity influences on the platinum atomic orbitals. Those orbitals containing significant platinum 6s character, which from symmetry arguments will be restricted to a_g and b_{3u} representations, are stabilized the most,

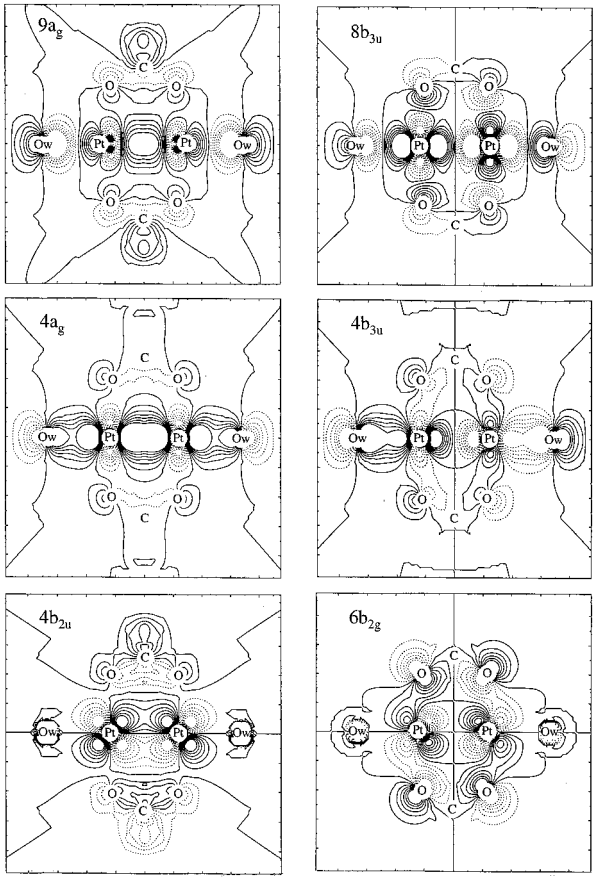

Figure 4. Contour maps for the orbitals involved in significant Pt−Pt bonding or antibonding interactions in $[Pt_2(O_2CH)_4(H_2O)_2]^{2+}$.

while those orbitals with significant platinum 5d character and little or no 6s character are raised in energy. Consequently, as in the case of $W_2(O_2CH)_4$, the relativistic correction leads to a strengthening of the metal−metal σ bond due to the additional stabilization of the $9a_g$ and $7a_g$ Pt−Pt σ bonding levels which contain approximately 8 and 5% platinum 6s character, respectively. In addition, the relativistic effect results in an appreciable destabilization of the $8b_{3u}(\sigma^*)$, $8a_g(\delta)$, $3b_{1g}(\pi^*)$, $4b_{2g}(\pi^*)$, $4b_{2u}(\pi)$, and $5b_{1u}(\pi)$ metal-based levels due to their high 5d character and absence of any significant 6s contribution.

Electronic Spectra

1. $[Rh_2(O_2CCH_3)_4(H_2O)_2]$. The electronic spectrum of $Rh_2(O_2CCH_3)_4(H_2O)_2$ has been examined by a number of workers.[18−22] Detailed low-temperature, polarized single-crystal, and MCD studies have been reported,[18,20,21] and more recently, CD spectra have been measured on closely related species.[22,23] On the basis of these measurements, the two lowest energy bands at approximately 17 000 (band A) and 22 500 cm^{-1} (band B) have been firmly established as the $\pi^*(Rh_2) \rightarrow \sigma^*(Rh_2)$ ($6b_{1g}$,$6b_{2g} \rightarrow 8b_{3u}$) and $\pi^*(Rh_2) \rightarrow \sigma^*(Rh-O)$ ($6b_{1g}$,$6b_{2g} \rightarrow 5a_u$) transitions. The calculated energies given in Table 4 for these two transitions are in very good agreement with the observed band positions. Furthermore, the calculated oscillator strengths (between 0.004 and 0.016) are very low, in line with the weak intensities observed for these transitions. In the solution spectrum, a weak higher energy shoulder (band C) is observed off band B at approximately 25 000 cm^{-1}. We assign this absorption to the $\delta(Rh_2) \rightarrow \sigma^*(Rh_2)$ ($9a_g \rightarrow 8b_{3u}$) transition which, from Table 4, is calculated at approximately 23 500 cm^{-1} with an oscillator strength less than 0.001.

The remaining transitions listed in Table 4, except the $8a_g \rightarrow 8b_{3u}$ ($\sigma(Rh_2) \rightarrow \sigma^*(Rh_2)$) and $6b_{1u}$,$5b_{2u} \rightarrow 6b_{3g}$ ($\pi(Rh_2) \rightarrow \sigma^*(Rh-O)$) transitions, all have a substantial component of ligand-to-metal charge-transfer (LMCT) character. We have recently examined in some detail the performance of the SCF−Xα−SW methodology in treating both LMCT and metal-based $\sigma \rightarrow \sigma^*$ transitions,[25,26] and concluded that the transition energy is substantially underestimated in both cases, but for rather different reasons. We have previously alluded to the tendency of the Xα−SW method to overestimate the stability of metal d orbitals, and this leads naturally to the conclusion that the energy of LMCT transitions should be underestimated. In metal hexahalides, the relationship between observed and calculated transition energies is systematic, with the latter too low by 7000−7500 cm^{-1} in all cases. While the nature of the metal−oxygen and metal−halide bonds may be somewhat different, our recent investigation of the MLCT bands in metal−acac complexes has indicated that the shortfall is similar to that in the metal−halide complexes. Consequently, an empirical correction factor, δ^{CT}, of 7500 cm^{-1} is added to all calculated CT transition energies.

Table 4. Calculated Transition Energies and Oscillator Strengths for all Electric Dipole Allowed Transitions under 50 000 cm^{-1} in $[Rh_2(O_2CH)_4(H_2O)_2]$

transition	ΔW (cm^{-1})	ΔE^{corr} (cm^{-1})	osc strength
$6b_{1g} \rightarrow 8b_{3u}$	17 720	17 720	0.006
$6b_{2g} \rightarrow 8b_{3u}$	19 280	19 280	0.004
$6b_{1g} \rightarrow 5a_u$	21 880	21 880	0.010
$6b_{2g} \rightarrow 5a_u$	23 390	23 390	0.016
$9a_g \rightarrow 8b_{3u}$	23 490	23 490	0.000
$8a_g \rightarrow 8b_{3u}$	27 140	36 290	0.422
$7b_{2u} \rightarrow 6b_{3g}$	32 610	40 110	0.190
$7b_{1u} \rightarrow 6b_{3g}$	33 740	41 240	0.282
$5b_{1g} \rightarrow 8b_{3u}$	34 270	41 770	0.030
$5b_{2g} \rightarrow 8b_{3u}$	36 010	43 510	0.026
$4b_{1g} \rightarrow 8b_{3u}$	36 190	43 690	0.019
$5b_{1g} \rightarrow 5a_u$	37 570	45 070	0.085
$4b_{2g} \rightarrow 8b_{3u}$	38 080	45 580	0.062
$3b_{1g} \rightarrow 8b_{3u}$	38 110	45 610	0.066
$5b_{2g} \rightarrow 5a_u$	38 530	46 030	0.070
$4b_{1g} \rightarrow 5a_u$	38 760	46 260	0.050
$4b_{2g} \rightarrow 5a_u$	40 640	48 140	0.147
$3b_{1g} \rightarrow 5a_u$	40 730	48 230	0.157
$6b_{2u} \rightarrow 6b_{3g}$	41 980	49 480	0.169
$7a_g \rightarrow 8b_{3u}$	42 110	49 610	0.113
$6b_{1u} \rightarrow 6b_{3g}$	43 460	43 460	0.157
$5b_{2u} \rightarrow 6b_{3g}$	44 150	44 150	0.126

The reason for the low energy calculated for the metal-based $\sigma \rightarrow \sigma^*$ transition energy has been traced to the neglect of electron correlation in the Xα wave function. Gray and co-workers[36] showed that the $\delta \rightarrow \delta^*$ transition in quadruply bonded M_2X_8 complexes could be described by the following equation

$$h\nu = K + (K^2 + \Delta W^2)^{1/2}$$

where K, the exchange integral, typically has a value between 6000 and 8000 cm^{-1}, ΔW is the calculated one-electron transition energy, and $h\nu$ is the observed transition energy. We have shown[25] that this equation is equally applicable to the metal-based $\sigma \rightarrow \sigma^*$ transition in metal nonahalides, M_2X_9. In Table 4, in addition to the raw calculated transition energies, ΔW, the corrected transition energies, ΔE^{corr} (adjusted to account for either CT or neglect of electron correlation as appropriate), are also shown.

The dominant feature of the spectrum in the high-energy region is an intense (ϵ = 17 000 M^{-1} cm^{-1}) band at approximately 45 500 cm^{-1} (band E) with a low-energy shoulder (band D) at 40 000 cm^{-1}, with an extinction coefficient of approximately 4000 M^{-1} cm^{-1}. The shoulder at 40 000 cm^{-1}

Table 5. Band Assignments for the Electronic Absorption Spectrum of $[Rh_2(O_2CH)_4(H_2O)_2]$

band	obsd position (cm^{-1})	calcd position (cm^{-1})	calcd osc strength	assignment[a]
A	17 100	17 720	0.006	$6b_{1g} \rightarrow 8b_{3u}$ $\pi^*(Rh_2) \rightarrow \sigma^*(Rh_2)$
		19 280	0.004	$6b_{2g} \rightarrow 8b_{3u}$ $\pi^*(Rh_2) \rightarrow \sigma^*(Rh_2)$
B	22 600	21 880	0.010	$6b_{1g} \rightarrow 5a_u$ $\pi^*(Rh_2) \rightarrow \sigma^*(Rh-O)$
		23 390	0.016	$6b_{2g} \rightarrow 5a_u$ $\pi^*(Rh_2) \rightarrow \sigma^*(Rh-O)$
C	25 000	23 500	<0.001	$9a_g \rightarrow 8b_{3u}$ $\delta(Rh_2) \rightarrow \sigma^*(Rh_2)$
D	40 000	36 290	0.422	$8a_g \rightarrow 8b_{3u}$ $\sigma(Rh_2) \rightarrow \sigma^*(Rh_2)$
		40 110	0.190	$7b_{2u} \rightarrow 6b_{3g}$ Ow $\rightarrow \sigma^*(Rh-O)$
		41 240	0.282	$7b_{1u} \rightarrow 6b_{3g}$ OAc $\rightarrow \sigma^*(Rh-O)$
E	45 000	43 460	0.157	$6b_{1u} \rightarrow 6b_{3g}$ $\pi(Rh_2) \rightarrow \sigma^*(Rh-O)$
		44 150	0.126	$5b_{2u} \rightarrow 6b_{3g}$ $\pi(Rh_2) \rightarrow \sigma^*(Rh-O)$
		45 070	0.085	$5b_{1g} \rightarrow 5a_u$ Ow $\rightarrow \sigma^*(Rh-O)$
		45 580	0.062	$4b_{2g} \rightarrow 8b_{3u}$ OAc $\rightarrow \sigma^*(Rh_2)$
		45 610	0.066	$3b_{1g} \rightarrow 8b_{3u}$ OAc $\rightarrow \sigma^*(Rh_2)$
		46 030	0.070	$5b_{2g} \rightarrow 5a_u$ OAc $\rightarrow \sigma^*(Rh-O)$
		46 260	0.050	$4b_{1g} \rightarrow 5a_u$ OAc $\rightarrow \sigma^*(Rh-O)$

[a] Orbital levels shown correspond to those determined for the formate complex.

has been previously assigned to the $\sigma(Rh_2) \rightarrow \sigma^*(Rh_2)$ transition by Norman and Kolari.[15] Later, Miskowski and co-workers[20] assigned this band to the $\sigma(Rh\text{-}O) \rightarrow \sigma^*(Rh_2)$ ($7a_g \rightarrow 8b_{3u}$) CT transition on the basis that the more intense band E was likely to be the $\sigma(Rh_2) \rightarrow \sigma^*(Rh_2)$ transition due to its narrowing and blue shift on cooling. The results in Table 4 do not support this latter assignment, as the $7a_g \rightarrow 8b_{3u}$ transition, after empirical adjustment, lies 10 000 cm^{-1} too high in energy. Even without the CT correction factor, there appears to be no reason to favor $7a_g \rightarrow 8b_{3u}$ over several other transitions with greater oscillator strengths which lie in the same region. Only three transitions are reasonable candidates for the shoulder at 40 000 cm^{-1}, namely, $8a_g \rightarrow 8b_{3u}$, $7b_{2u} \rightarrow 6b_{3g}$, and $7b_{1u} \rightarrow 6b_{3g}$, although it is possible that the latter two transitions are contributing to band E instead. The former transition corresponds to $\sigma(Rh_2) \rightarrow \sigma^*(Rh_2)$, while the latter two transitions have predominantly Ow $\rightarrow$ Rh and OAc $\rightarrow$ Rh CT character, respectively. Although the full δ^{CT} correction factor of 7500 cm^{-1} has been applied to the $7b_{2u} \rightarrow 6b_{3g}$ and $7b_{1u} \rightarrow 6b_{3g}$ transitions, it is likely to be less than this on the basis of the donor and acceptor orbital compositions given in Table 3. From the calculated oscillator strengths given in Table 4, it would appear that the $\sigma(Rh_2) \rightarrow \sigma^*(Rh_2)$ transition should dominate the shoulder at 40 000 cm^{-1}. However, we have previously found that the Xα−SW method significantly overestimates the intensity of metal-based $\sigma \rightarrow \sigma^*$ transitions,[25] again, presumably the result of the neglect of electron correlation in the Xα−SW wave function. Given this, the possibility that the Ow $\rightarrow$ Rh and OAc $\rightarrow$ Rh CT transitions also contribute significantly to the absorption in this region cannot be ruled out.

On the basis of Table 4, the more intense higher energy absorption (band E), observed at approximately 45 500 cm^{-1}, can be attributed to a number of CT transitions of moderate intensity calculated between 43 000 and 46 500 cm^{-1}. The $6b_{1u}$,$5b_{2u} \rightarrow 6b_{3g}$ ($\pi(Rh_2) \rightarrow \sigma^*(Rh-O)$) transitions are also included in this assignment, but their calculated transition energies have not been adjusted by δ^{CT} since, in both cases, the donor and acceptor orbitals are of very similar composition. The proposed assignments for the spectrum of $Rh_2(OAc)_4(H_2O)_2$ are summarized in Table 5.

2. $[Pt_2(O_2CCH_3)_4(H_2O)_2]^{2+}$. It was not possible to measure directly the absorption spectrum of $[Pt_2(O_2CCH_3)_4(H_2O)_2]^{2+}$ in solution due to its limited stability in most solvents. The only solvent in which the species was relatively stable was dmf, but even in this case, NMR studies[4] have shown that the

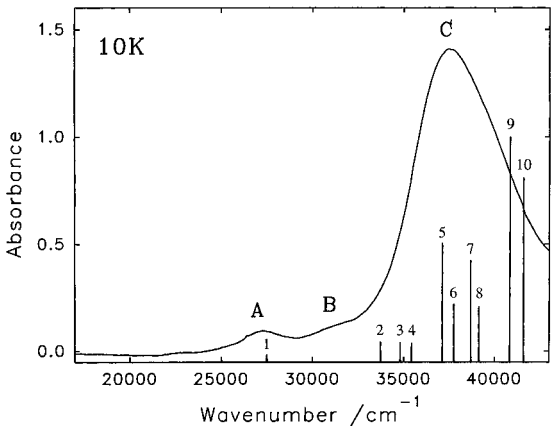

Figure 5. Low-temperature absorption spectrum of $[Pt_2(O_2CCH_3)_4(H_2O)_2]^{2+}$. The X$\alpha$−SW calculated transition energies and relative intensities (based on the $7b_{1u} \rightarrow 6b_{3g}$ transition being assigned an arbitrary absorbance of 1.0) are shown in the form of a stick diagram. The numbering scheme corresponds to (1): $6b_{1g} \rightarrow 8b_{3u}$; (2) $6b_{2g} \rightarrow 8b_{3u}$; (3) $5b_{1g} \rightarrow 8b_{3u}$; (4) $6b_{1g} \rightarrow 5a_u$; (5) $9a_g \rightarrow 8b_{3u}$; (6) $6b_{2g} \rightarrow 5a_u$; (7) $7b_{2u} \rightarrow 6b_{3g}$; (8) $5b_{1g} \rightarrow 5a_u$; (9) $7b_{1u} \rightarrow 6b_{3g}$; (10) $6b_{2u} \rightarrow 6b_{3g}$.

$[Pt_2(O_2CCH_3)_4(H_2O)_2]^{2+}$ species exists in equilibrium with the mono- and di-substituted dmf species, $[Pt_2(O_2CCH_3)_4(H_2O)(dmf)]^{2+}$ and $[Pt_2(O_2CCH_3)_4(dmf)_2]^{2+}$, respectively, with the mono-substituted dmf species predominant at concentrations typically used for UV/vis spectra ($\sim 10^{-4}$ M). Furthermore, the strong UV absorption band(s) are largely obscured by the intense absorption of the dmf solvent above approximately 37 000 cm^{-1}. However, we have previously observed that nafion film, a perfluoro based cation exchange membrane, is often selective in the species it takes up from a solution equilibrium. In light of this, we placed nafion film in a concentrated solution of the triflate salt of $[Pt_2(O_2CCH_3)_4(H_2O)_2]^{2+}$ in dmf in the hope that the film would preferentially take up the diaqua complex rather than the mono- or di-substituted dmf species.

The low-temperature (10 K) absorption spectrum of $[Pt_2(O_2CCH_3)_4(H_2O)_2]^{2+}$ in nafion film is shown in Figure 5. The nafion film spectrum clearly resolves the strong UV absorption (band C) which is obscured in the room temperature dmf solution spectrum due to an intense solvent absorption. Furthermore, the lowest energy band, which occurs at approximately 25 000 cm^{-1} in the dmf solution spectrum, moves to $\sim$27 500 cm^{-1} in the nafion film spectrum. A more concentrated nafion film spectrum highlighting the lowest energy band revealed two weak lower energy shoulders at approximately 25 000 and 23 500 cm^{-1}. The former corresponds to the position of the lowest energy band observed in the dmf solution spectrum, which is predominantly the mono-substituted dmf species, while the latter may be due to the di-substituted dmf species. The dominant higher energy component at $\sim$27 500 cm^{-1} must therefore be attributed to the desired diaqua species. Consequently, it can be concluded that the nafion film has preferentially taken up the diaqua species with apparently only minor uptake of the mono- and di-substituted dmf species.

On the assumption that the low-temperature nafion film spectrum shown in Figure 5 is predominantly due to the $[Pt_2(O_2CCH_3)_4(H_2O)_2]^{2+}$ species, assignments for the observed bands can be made on the basis of the Xα−SW calculated transition-state energies and oscillator strengths reported in Table 6. Once again, CT transitions are defined as those transitions arising from orbitals with less than 35% metal character and are empirically corrected by δ^{CT} in Table 6, except where the donor and acceptor orbitals are of similar composition. It should be noted, however, that the more extensive mixing of metal and ligand character in the diplatinum system makes the

Table 6. Calculated Transition Energies and Oscillator Strengths for all Electric Dipole Allowed Transitions under 50 000 cm^{-1} in $[Pt_2(O_2CH)_4(H_2O)_2]^{2+}$

transition	ΔW (cm^{-1})	ΔE^{corr} (cm^{-1})	osc strength
$6b_{1g} \rightarrow 8b_{3u}$	20 080	27 580	0.021
$6b_{2g} \rightarrow 8b_{3u}$	26 300	33 800	0.059
$5b_{1g} \rightarrow 8b_{3u}$	27 490	34 990	0.058
$6b_{1g} \rightarrow 5a_u$	28 000	35 500	0.054
$9a_g \rightarrow 8b_{3u}$	28 650	37 190	0.356
$8a_g \rightarrow 8b_{3u}$	29 690	29 690	0.000
$6b_{2g} \rightarrow 5a_u$	30 380	37 880	0.172
$7b_{2u} \rightarrow 6b_{3g}$	31 270	38 770	0.305
$5b_{1g} \rightarrow 5a_u$	31 670	39 170	0.166
$5b_{2g} \rightarrow 8b_{3u}$	31 850	39 350	0.004
$4b_{1g} \rightarrow 8b_{3u}$	31 970	39 470	0.009
$7b_{1u} \rightarrow 6b_{3g}$	33 340	40 840	0.679
$6b_{2u} \rightarrow 6b_{3g}$	34 120	41 620	0.558
$5b_{2g} \rightarrow 5a_u$	34 990	42 490	0.012
$4b_{1g} \rightarrow 5a_u$	35 270	42 770	0.025
$4a_u \rightarrow 6b_{3g}$	36 970	44 470	0.000
$4b_{2g} \rightarrow 8b_{3u}$	37 960	37 960	0.043
$7a_g \rightarrow 8b_{3u}$	38 860	46 360	0.401
$3b_{1g} \rightarrow 8b_{3u}$	38 900	38 900	0.034
$4b_{2g} \rightarrow 5a_u$	42 760	42 760	0.073
$3b_{1g} \rightarrow 5a_u$	43 890	43 890	0.068

distinction between CT and non-CT transitions less clear. We will return to this important point later in the discussion.

The lowest energy band at 27 000 cm^{-1} (band A) with ϵ = 1500 M^{-1} cm^{-1} is readily assigned to the $6b_{1g} \rightarrow 8b_{3u}$ transition, which, after empirical correction by δ^{CT}, is calculated to lie at 27 580 cm^{-1}. This transition is almost entirely Ow $\rightarrow \sigma^*(Pt_2)$ in nature, but the Ow lone pair lies perpendicular to the Pt−Pt axis. It is consequently inefficiently orientated for overlap with the Ow component of the $8b_{3u}$ orbital, which lies along the Pt−Pt axis, and the resultant oscillator strength is very low. A very weak transition is observed at ∼22 500 cm^{-1}, which we assign to the corresponding spin−triplet transition which is expected to be some 3000−5000 cm^{-1} lower in energy than the spin−singlet transition.[12]

From Table 6, a series of more intense transitions are predicted to commence at approximately 34 000 cm^{-1}, reaching an intensity maximum in the region of 41 000 cm^{-1}. This pattern fits reasonably well with the observed spectrum, with the shoulder at 31 500 cm^{-1} (band B) being attributed to the lowest energy $6b_{2g}$, $5b_{1g} \rightarrow 8b_{3u}$ (OAc $\rightarrow \sigma^*(Pt_2)$) and $6b_{1g} \rightarrow 5a_u$ (Ow $\rightarrow \sigma^*$(Pt-O)) LMCT transitions. However, it is noted that the $6b_{2g}$, $5b_{1g} \rightarrow 8b_{3u}$ transitions are partially $\pi^*(Pt_2) \rightarrow \sigma^*(Pt_2)$ in character, and, given that the $6b_{2g}$ and $5b_{1g}$ donor orbitals, on average, are of approximately 25% Pt composition, the distinction between CT and d−d character is somewhat blurred. Consequently, the CT energy correction may be attenuated for these two transitions with the result that they may be contributing to band A rather than band B. The MCD observed for band A is also consistent with this assignment. Even if this latter assignment is correct, the calculations still indicate that the $6b_{2g}$, $5b_{1g} \rightarrow 8b_{3u}$ transitions will have significant LMCT character in contrast with the analogous $6b_{1g}$, $6b_{2g} \rightarrow 8b_{3u}$ ($\pi^*(Rh_2) \rightarrow \sigma^*(Rh_2)$) transitions in the Rh(II) complex, which are largely metal localized.

The most intense feature of the spectrum, band C, is attributed largely to OAc $\rightarrow \sigma^*$(Pt−O) and Ow $\rightarrow \sigma^*$(Pt−O) LMCT transitions. The $9a_g \rightarrow 8b_{3u}$ transition is also predicted to contribute to this band which is of some interest, because, as shown in Figure 4a (top, left) there is significant (26%) Pt−Pt σ character in the donor orbital. In Table 6, the transitions were somewhat arbitrarily separated into two categories, CT and non-CT, on the basis of the donor orbital composition, and while the $9a_g \rightarrow 8b_{3u}$ is indeed predominantly CT in nature, it also contains considerable $\sigma(Pt_2) \rightarrow \sigma^*(Pt_2)$ character. The decreased LMCT character might be expected to reduce the effect of the CT correction, thereby reducing the true transition energy below that given by $\Delta W + \delta^{CT}$. However, at the same time as the CT character of the transition is reduced, the σ(Pt) $\rightarrow \sigma^*$(Pt) component is increased, and the effects of electron correlation, as embodied in the above equation, become more significant. Thus, we suggest that the difference between calculated and observed transition energies will be relatively insensitive to changes in the proportion of σ(Pt) $\rightarrow \sigma^*$(Pt) and LMCT character.

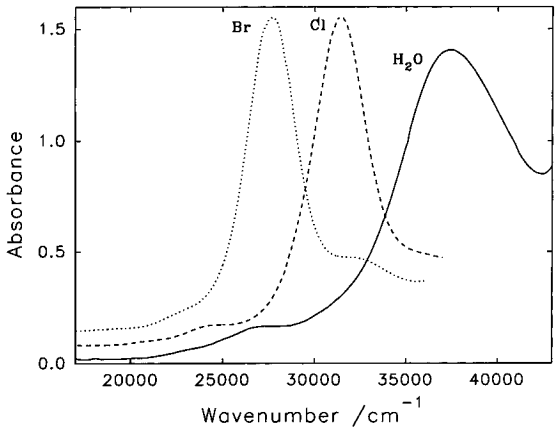

Figure 6. Comparison of room temperature absorption spectra for $[Pt_2(O_2CCH_3)_4L_2]^{n+}$ (L = H_2O, Cl, Br).

Table 7. Band Assignments for the Electronic Absorption Spectrum of $[Pt_2(O_2CH)_4(H_2O)_2]^{2+}$

band	obsd position (cm^{-1})	calcd position (cm^{-1})	calcd osc strength	assignment[a]
A	27 500	27 580	0.021	$6b_{1g} \rightarrow 8b_{3u}$ Ow $\rightarrow \sigma^*(Pt_2)$
B	31 500	33 800	0.059	$6b_{2g} \rightarrow 8b_{3u}$ OAc $\rightarrow \sigma^*(Pt_2)$
		34 990	0.058	$5b_{1g} \rightarrow 8b_{3u}$ OAc $\rightarrow \sigma^*(Pt_2)$
		35 500	0.054	$6b_{1g} \rightarrow 5a_u$ Ow $\rightarrow \sigma^*$(Pt−O)
C	37 500	37 190	0.356	$9a_g \rightarrow 8b_{3u}$ $\sigma(Pt_2) \rightarrow \sigma^*(Pt_2)$
		37 880	0.172	$6b_{2g} \rightarrow 5a_u$ OAc $\rightarrow \sigma^*$(Pt−O)
		38 770	0.305	$7b_{2u} \rightarrow 6b_{3g}$ Ow $\rightarrow \sigma^*$(Pt−O)
		39 170	0.166	$5b_{1g} \rightarrow 5a_u$ OAc $\rightarrow \sigma^*$(Pt−O)
		40 840	0.679	$7b_{1u} \rightarrow 6b_{3g}$ OAc $\rightarrow \sigma^*$(Pt−O)
		41 620	0.558	$6b_{2u} \rightarrow 6b_{3g}$ OAc $\rightarrow \sigma^*$(Pt−O)

[a] Orbital levels shown correspond to those determined for the formate complex.

Figure 6 indicates that the energy of band C is markedly sensitive to the nature of the axial ligand, exhibiting a dramatic shift to lower energy as the axial substituents are changed from H_2O to Cl and Br. This change is consistent with the significant axial-ligand CT character associated with the $9a_g \rightarrow 8b_{3u}$ and $7b_{2u} \rightarrow 6b_{3g}$ transitions which contribute to this band. The broadness and asymmetry of this band in the diaqua complex also implies the presence of more than one component, and indeed, as discussed above, there are several OAc $\rightarrow \sigma^*$(Pt−O) LMCT transitions of significant intensity predicted in this region. Thus, unlike the spectra of the axial halide adducts, the intensity of band C for the diaqua complex cannot be attributed solely to the $\sigma(Pt_2,L) \rightarrow \sigma^*(Pt_2)$ transition. The spectral assignments for $[Pt_2(O_2CCH_3)_4(H_2O)_2]^{2+}$ are summarized in Table 7.

3. $[Pt_2(SO_4)_4(H_2O)_2]^{2-}$ and $[Pt_2(HPO_4)_4(H_2O)_2]^{2-}$. As noted previously, the absorption spectrum of $Pt_2(O_2CCH_3)_4L_2$ (L = Cl, Br, H_2O) complexes are very similar to the analogous sulfate (SO_4^{2-}) and hydrogen phosphate (HPO_4^{2-}) bridged complexes of platinum(III). Consequently, the above assignments for $[Pt_2(O_2CCH_3)_4(H_2O)_2]^{2+}$ should be transferable to

$[Pt_2(SO_4)_4(H_2O)_2]^{2-}$ and $[Pt_2(HPO_4)_4(H_2O)_2]^{2-}$ complexes. In both the sulfate and hydrogen phosphate complexes, bands are observed at approximately 26 000 cm^{-1} ($\epsilon \sim 700$ M^{-1} cm^{-1}) and 44 500 cm^{-1} ($\epsilon \sim 25\,000$ M^{-1} cm^{-1}), while a lower energy shoulder is also apparent in the spectrum of the sulfate complex at ~38 500 cm^{-1}.[12-14] The weaker band at 26 000 cm^{-1} has been previously assigned to the $\pi^*(Pt_2) \rightarrow \sigma^*(Pt_2)$ transition, in agreement with the observed MCD for this band.[14] The assignment proposed in Table 7 for $[Pt_2(O_2CCH_3)_4(H_2O)_2]^{2+}$ is equally in accord with the observed MCD but suggests a large component of LMCT character in this transition. The lower energy shift of this band (~4500 cm^{-1}) with a change in the axial ligand from H_2O to Cl and Br is around half that observed for the intense UV absorption (band C), consistent with the LMCT character of this transition.

The intense band at 44 500 cm^{-1} was previously assigned to the $\sigma(L) \rightarrow \sigma^*(Pt_2)$ transition due to the significant axial ligand character mixed into the $\sigma(Pt_2)$ orbital, but this assignment was recently shown to be in conflict with the observed MCD.[14] However, based on the above assignments for the $[Pt_2(O_2CCH_3)_4(H_2O)_2]^{2+}$ complex, a number of excited states are expected to contribute to the intensity of this band, including the $\sigma(L) \rightarrow \sigma^*(Pt_2)$ transition. The MCD for this band, on the other hand, cannot be due to this transition, as the negative A term observed in the MCD spectrum indicates the presence of a degenerate excited state. The most obvious choice, based on the predicted MCD signs using the one-center approximation,[14] are the $SO_4 \rightarrow \sigma^*(Pt-O)$ or $PO_4 \rightarrow \sigma^*(Pt-O)$ LMCT transitions, corresponding to the ($6b_{2g}$, $5b_{1g} \rightarrow 5a_u$) or ($7b_{1u}$, $6b_{2u} \rightarrow 6b_{3g}$) transitions in the analogous formate complex, which are predicted to lie in the vicinity of this band with relatively large intensities.

The electronic structure calculations for the $[Pt_2(O_2CH)_4(H_2O)_2]^{2+}$ complex thus lead to a rational solution to the previously contradictory MCD spectra for the intense UV band in the sulfate and hydrogen phosphate complexes. As with the platinum(III) acetate complex, the intensity of the strong UV band results from a number of transitions, one of which has significant $\sigma(Pt_2) \rightarrow \sigma^*(Pt_2)$ character. The MCD for this band, however, arises from $SO_4 \rightarrow \sigma^*(Pt-O)$ or $PO_4 \rightarrow \sigma^*(Pt\text{-}O)$ LMCT transitions.

Finally, the lower energy shoulder observed at approximately 38 500 cm^{-1} in the sulfate complex is coincident with the strong UV band in the spectrum of the acetate complex. Given the close correspondence of the lower energy transitions in the sulfate and acetate complexes, it is tempting to assign this shoulder to the equivalent of the $9a_g \rightarrow 8b_{3u}$ transition in the formate complex which has a significant $\sigma(Pt_2) \rightarrow \sigma^*(Pt_2)$ component, while the higher energy portion of the band at approximately 44 000 cm^{-1} is attributed mainly to $SO_4 \rightarrow \sigma^*(Pt-O)$ LMCT transitions.

IC9506015